Proceedings World Geothermal Congress 2020+1
Reykjavik, Iceland, April - October 2021

# Quick and Preliminary Approach for Forecasting Natural Recharge to a Hydrothermal Reservoir During Production

Mitsuo Matsumoto

Department of Earth Resources Engineering, Faculty of Engineering, Kyushu University,
744, Motooka, Nishi-ku, Fukuoka 819-0395, Japan

matsumoto@mine.kyushu-u.ac.jp

**Keywords:** forecasting future production rates, natural recharge, production test, reservoir simulation

**ABSTRACT**

This study proposes a quick and preliminary approach for forecasting natural recharge to a hydrothermal reservoir during a long production period—spanning over a few tens of years. This approach determines the frequency distributions of the pressure decline and production rate after an arbitrary period of production, based on observations of pressure transients during production tests. A case study which assumed a planar reservoir demonstrated an example of this approach. Investigations revealed the dependency of the simulated frequency distribution of the production rate on several conditions as well as how extending the duration of a production test improved the precision of forecasting future production rates.

## 1. INTRODUCTION

Sustainable development of geothermal energy is essential in order to maximize the benefits of geothermal resources, and also to remain successful in the geothermal industry. A key element for achieving sustainability is the conservation of mass balance in geothermal reservoirs by extracting geothermal fluid within the capacity of natural recharge. In general, a geothermal reservoir is part of a huge and complex hydrothermal system including extensively from the ground surface to a deep heat source. An accepted and standard approach for forecasting the natural recharge during a production period spanning a few tens of years is to comprehensively study the system through extensive exploration and modeling; these models commonly include natural-state models and history matching (e.g., Grant and Bixley, 2011; DiPippo, 2008).

This study aims to construct a quick and preliminary approach for forecasting the natural recharge in not only a quantitative manner, but also by taking into account the uncertainty of the forecast through frequency distributions of pressure declines and production rates. The advantage of this approach is that it provides us with quantitative estimates that are useful in evaluating project feasibility of geothermal industries at an early stage, based on simple assumptions and interpretations of observations of pressure transients during production tests. In this study, we first present the concepts of the approach, including the theoretical background. Next, we demonstrate a simple case study assuming a planar reservoir. Finally, we investigate the dependency of the simulated frequency distribution of the production rate on several conditions.

## 2. CONCEPTS

Let us consider a circular and planar reservoir with a radius of $r_{\mathrm{e}}$ containing liquid water. A production well penetrates the center of this reservoir and extracts the fluid at a constant volumetric flow rate. Consistent with the classical theory of well test analysis (e.g., Dake et al., 1978), the temporal pressure changes at the external boundary of the reservoir and the feed zone of the production well vary depending on the natural recharge into the reservoir across the external boundary after the radius of investigation $r_{\mathrm{inv}}(t)$ reaches this boundary ($r_{\mathrm{inv}}(t) = r_{\mathrm{e}}$).

### 2.1 Quantifying the Natural Recharge by Defining Imaginary Region

Figure 1 schematically illustrates the temporal pressure changes taking place during production at a constant volumetric flow rate on a logarithmic scale corresponding to several cases of natural recharge. These pressure changes are at the external boundary of the reservoir as well as the feed zone of the production well. We can define the most optimistic case that assumes a constant boundary pressure maintained at the initial value distributing uniformly throughout the initial reservoir. This case assumes that the recharge rate finally converges on the production rate resulting in steady state. In contrast, the most pessimistic case assumes an impermeable boundary that allows no recharge. In this case, the pressure declines proportionally with real time. The slope of this proportional decline depends on the reservoir volume and volumetric production rate. When shown on a logarithmic time scale as in Figure 1, the pressure drops non-linearly.

The real cases should occur between the most optimistic and pessimistic cases. One probable pressure change is the simple extrapolation of the linear decrease in the feed zone pressure on the logarithmic time scale (Figure 1). In this case, the pressure at the external boundary also begins to decrease at the same rate after the radius of investigation passes the external boundary. This condition can be reproduced theoretically by assuming an imaginary region extending infinitely outside the reservoir (Figure 2). The imaginary region in this case has the same values of transmissivity and storativity as the inside of the reservoir. By modifying these parameters in the imaginary region, we can control the natural recharge continuously between the most optimistic and pessimistic cases. Assuming a moderate value of the storativity, the most optimistic case assumes an infinitely large transmissivity, while the most pessimistic case assumes that the transmissivity is zero.

Typical real and successfully developed reservoirs are open systems. They are part of a huge and complex hydrothermal system including extensively from the ground surface to a deep heat source. Because it is difficult to clearly define the external boundary

of such reservoirs, we define the reservoir as the region already investigated during production tests (i.e., $r_e$=$r_{inv}(t)$ at $\forall t$). Because the radius of investigation depends on time, the external boundary of the reservoir advances outwards with the passage of time. The transmissivity and storativity in the reservoir can be estimated from the pressure transients observed during the production tests. However, the accurate three-dimensional shape of a heterogeneously distributing real reservoir can rarely be determined, and we have only observations of pressure transients during some time period. This means that the radius of investigation is only valid as a 'distance' in the theoretically assumed reservoir that extends radially and uniformly from the production well and is consistent with the observed pressure transients. We can rarely apply the radius of investigation to a real distance on the field map.

In the case of a reservoir with an arbitrary shape, as is often assumed in practical numerical simulation models, the external boundary of the reservoir is still defined by the region already investigated during production tests. We can find the location of this boundary by searching the distribution of numerical blocks or grid points at which trial modifications of transmissivity or storativity affect the match between the simulated and observed pressure transient data of the production tests. If the trial modification of these parameters at a numerical block never affect the agreement between simulated and observed transients, the location of this block is deemed to be outside the investigated region during the production tests (i.e., outside the reservoir).

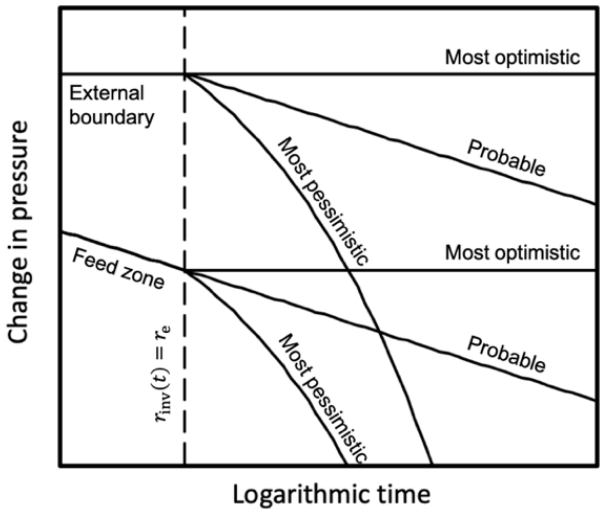


**Figure 1: Schematic representation of pressure changes at the external boundary of the reservoir and the feed zone of the production well during production at a constant volumetric flow rate.**

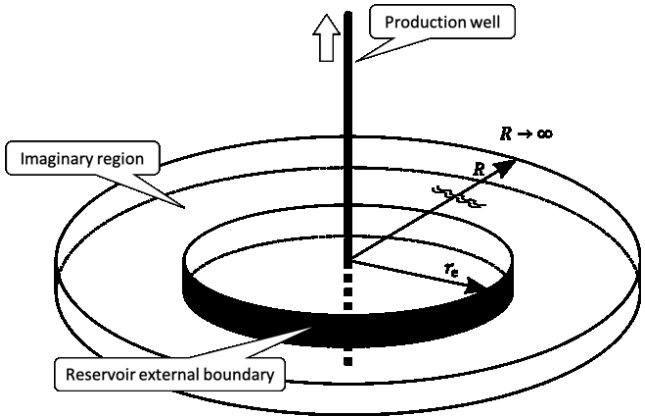


**Figure 2: Planar reservoir model surrounded by an imaginary region controlling the natural recharge into the reservoir across the external boundary.**

### 2.2 Monte Carlo Approach for Forecasting Natural Recharge

The natural recharge to the reservoir across the external boundary has been quantified by defining the transmissivity and storativity in the imaginary region, upon which the recharge rate becomes amenable to mathematical control. By taking advantage of this fact, let us forecast the natural recharge during a production period spanning over a few tens of years, based on a production test. We adopted a Monte Carlo approach for this forecast.

As discussed above (Figure 1), we can forecast one probable pressure change at the feed zone of the production well by extrapolating the pressure change that corresponds to the transmissivity and storativity values already determined from observations

of the pressure transients. Above and below this probable case, we define a range of probable pressure changes as illustrated in Figure 3. The upper and lower limits of this range are assumed arbitrarily but can never be higher and lower than the most optimistic and pessimistic cases, respectively. The range of these pressure changes is described by the ranges of transmissivity and storativity in the imaginary region. Generating random numbers that conform to the assumed probability distribution functions of these parameters, we can apply the Monte Carlo approach to forecasting the pressure change as well as the natural recharge to the reservoir during a long production period. The result of the Monte Carlo approach generates the frequency distributions of the simulated results, including the reservoir pressure decline that occurs under an assumed production rate, and the production rate under an assumed wellhead pressure and wellbore flow model.

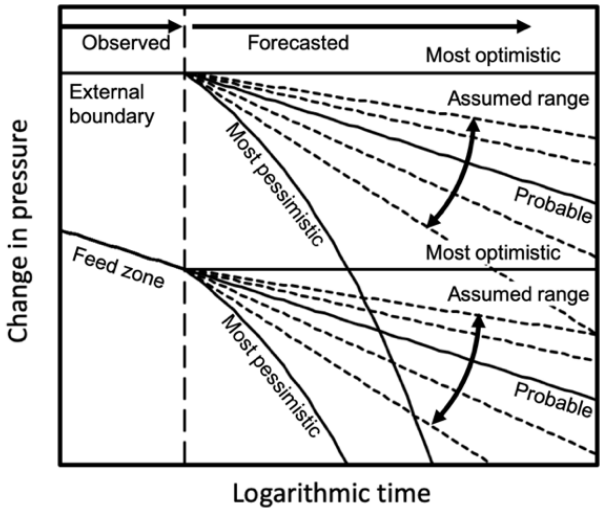


**Figure 3: Schematic representation of forecasted pressure changes at the external boundary of the reservoir and the feed zone of the production well during production at a constant volumetric flow rate. Note that the pressure changes during the 'observed' interval are not observed directly but calculated, based on the transmissivity and storativity values that were determined from observed pressure transients during a production test. The length of the 'observed' interval is constrained by the duration of the production test.**

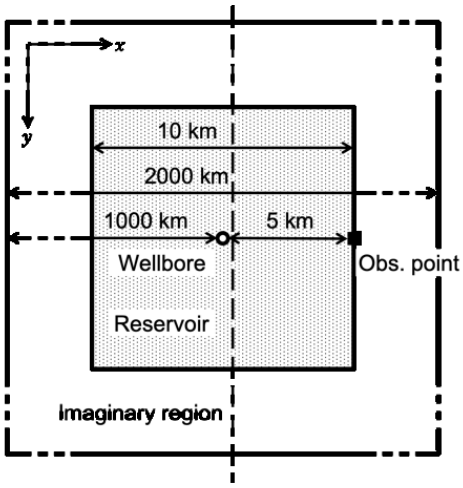


**Figure 4: Numerical model of a square and horizontal reservoir with sides of 10 km surrounded by an imaginary region with sides of 2000 km. In Section 4.2, the imaginary region is divided into two parts along the broken line 385 m in the $x$-direction from the wellbore.**

## 3. CASE STUDY: A PLANAR RESERVOIR

### 3.1 Conditions

Let us consider production from a square and horizontal reservoir having sides measuring 10 km, as shown in Figure 4. A wellbore penetrates at the central point, located 5 km from each side. The initial values of pressure and specific enthalpy in the reservoir are uniform at 8 MPa and 950 kJ/kg, respectively. We assume that the transmissivity is $8.17 \times 10^{-8}$ m$^3$ Pa$^{-1}$ s$^{-1}$, and the storativity is $1.11 \times 10^{-8}$ m Pa$^{-1}$ in the reservoir, which have been already determined from a production test. An imaginary region extends outside this reservoir. In order to represent an infinite extension numerically, the external boundary of this imaginary region is

assumed to be 1000 km away from the wellbore, thus forming a square having sides of 2000 km. This external boundary is therefore sufficiently far away within the time interval of the numerical solutions shown below. The initial values of pressure and specific enthalpy in the imaginary region are the same as those in the reservoir. At the external boundary of the imaginary region, pressure and specific enthalpy are constant at these initial values throughout the simulations, although selection of the external boundary condition of the imaginary region never affects the numerical solutions.

During numerical simulations, we adopted the extended version of the numerical code described by Matsumoto (2018). This code implements a highly refined local grid in the vicinity of the wellbore that seamlessly connects the numerical flow model in the wellbore and the global grid covering the total reservoir. Thus, we can accurately simulate pressure changes in the wellbore during production. The extension includes the implementation of random modifications to the permeability (i.e., transmissivity) of the imaginary region, while ensuring conformation to the uniform probability distribution function on the logarithmic scale. The upper and lower domain limits of this function can be selected as an input parameter. In this study, the storativity in the imaginary region was assumed to be constant and equal to that in the reservoir, for the sake of simplicity.

The grid size in the reservoir is uniform at 385 m in the $x$- and $y$-directions, while that in the imaginary region is exponentially expanded to 491 km with the distance from the wellbore. In the local grid, the grid size also expands exponentially from 1 mm at the point of contact with the wellbore surface, to 215 m at the external boundary, where the pressure values contained in the local and global grids are transferred to each other. The total numbers of grid points in the $x$- and $y$-directions are 51 in the global grid, while those in the radial ($r$-) and circumferential ($\theta$-) directions are 41 and 10, respectively. This includes the grid points that are overwrapped in order to represent the periodic boundary condition at $\theta = 0$ [rad]. The magnitude of the time step size expands exponentially from 7.01 s to 7.89 h for the first year and becomes constant thereafter (throughout the following nine years). The total number of time steps for the entire ten years is 20000.

### 3.2 Numerical solutions

3.2.1 Production at a Constant Rate

First, we assumed production at a constant mass flow rate of 200 t/h. Because the fluid in the reservoir is liquid water with low compressibility, this can be regarded as equivalent to a constant volumetric flow rate of $6.58 \times 10^{-2}$ m$^3$ s$^{-1}$, assuming a fluid density of 844 kg m$^{-3}$ corresponding to the initial reservoir conditions. The total number of simulations conducted was 120 with different transmissivities in the imaginary region; these were randomly chosen across four orders of magnitude, from $8.17 \times 10^{-10}$ to $8.17 \times 10^{-6}$ m$^3$ Pa$^{-1}$ s$^{-1}$.

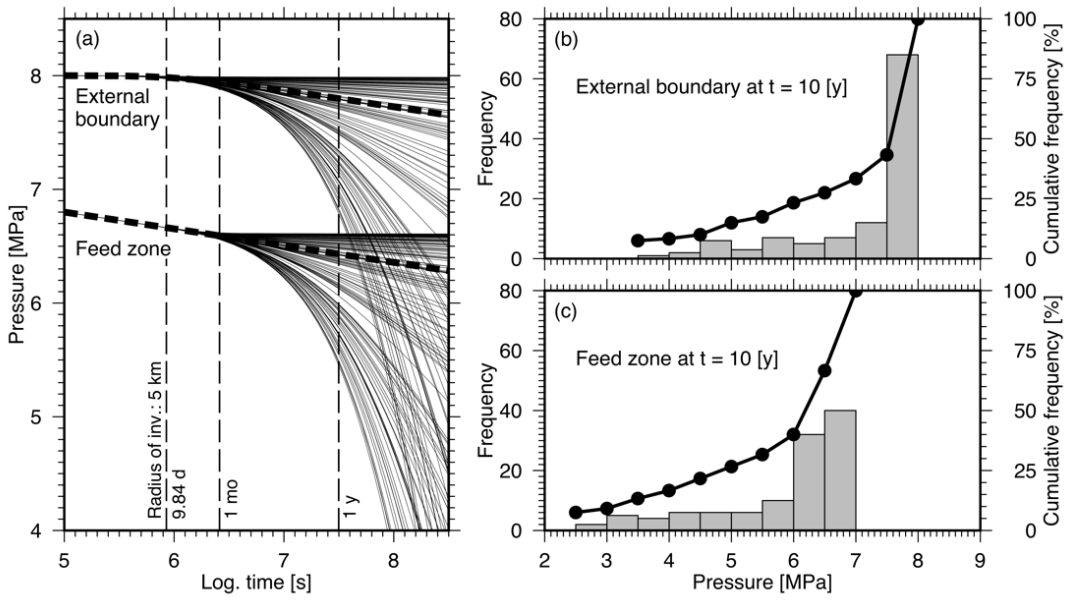


**Figure 5: Pressure changes with a constant production rate. (a) Temporal changes at the external boundary of the reservoir and the feed zone of the production well for all 120 simulations. The thick broken line represents the probable case. (b, c) Frequency distributions at the external boundary and feed zone at the end of the simulations (10 y) (with the exception of the nine simulations that stopped before the assumed end time of 10 y). Note that the lower-most values of the cumulative frequency are not zero because these nine simulations were accounted for.**

Figure 5 summarizes the pressure changes at the external boundary of the reservoir 5000 m from the production well ('Obs. point' in Figure 4) as well as at the feed zone of the production well, for all 120 simulations. The probable case without modifying the transmissivity is also shown for reference. The pressure changes varied after the radius of investigation passed the external boundary. The differences in these pressure changes were very small for the first one month, but they became more prominent after one year had lapsed (Figure 5a). Nine simulations ceased before reaching the assumed end time of 10 y because the feed zone pressure became lower than the boiling pressure of 2.381 MPa. The numerical code is not currently capable of simulating two-

phase problems. With the exception of these nine simulations, the frequencies of the pressure at the external boundary of the reservoir and the feed zone of the production well at the end of the simulations (10 y) tended to be higher near the upper limit of each frequency distribution (Figure 5b, c). This was because the range of modified transmissivities was selected by assuming equal probabilities above and below the value of the probable case. The transmissivity assumed in the probable case ($8.17 \times 10^{-8}$ $m^3$ $Pa^{-1}$ $s^{-1}$) is relatively high and comparable to the most optimistic case assuming infinite transmissivity. This resulted in a dense distribution of pressure within the interval between the probable and most optimistic cases.

3.2.2 Production at a Constant Wellhead Pressure

Next, we assumed production at a constant wellhead pressure, as applied by Matsumoto (2018) using a wellbore flow model. This model provides a relationship between the mass flow rate and feed zone pressure derived empirically by computing under a constant wellhead pressure. Thus, the production rate ranged from 9.47 to 620 t/h, depending on the feed zone pressure, which ranged from 3 to 9 MPa. The total number of simulations conducted was 120 with randomly modified transmissivities, as described above.

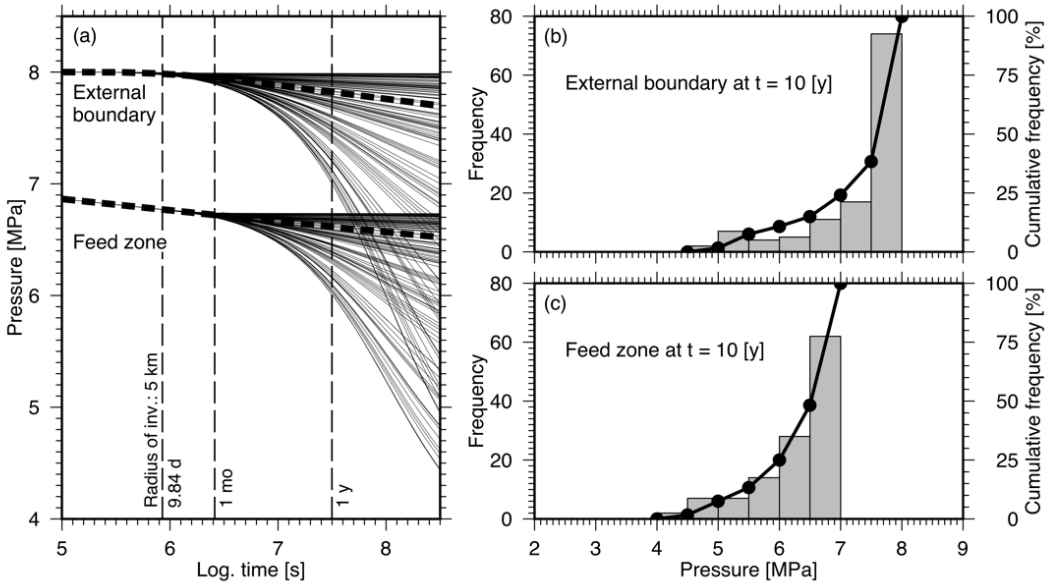


**Figure 6: Pressure changes assuming a constant wellhead pressure. (a) Temporal changes at the external boundary of the reservoir and the feed zone of the production well for all 120 simulations. The thick broken line represents the probable case. (b, c) Frequency distributions at the external boundary and feed zone at the end of the 120 simulations (10 y).**

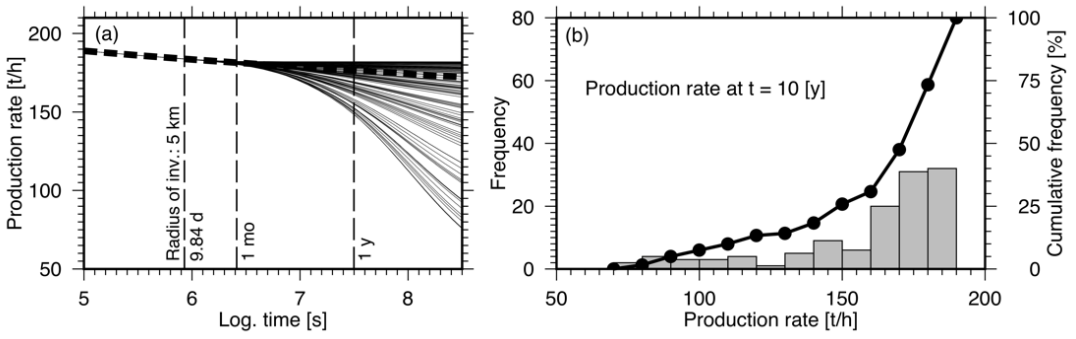


**Figure 7: Changes in the production rate assuming a constant wellhead pressure. (a) Temporal changes for all 120 simulations. The thick broken line represents the probable case. (b) Frequency distribution at the end of the 120 simulations (10 y).**

Figure 6 summarizes the pressure changes at the external boundary of the reservoir 5000 m from the production well (Obs. point in Figure 4), as well as at the feed zone of the production well, for all 120 simulations. With a constant wellhead pressure, the pressure drops tended to be gentler than those observed with a constant production rate (Figure 6a). This was because the production rate was reduced, effectively conforming to the relationship with feed zone pressure when the transmissivity in the imaginary region was occasionally small. Consequently, the frequency distributions of the pressure at the external boundary of the reservoir and the

feed zone of the production well exhibited a smaller extension toward smaller values than those of a constant production rate (Figure 6b, c). All simulations continued until the assumed end time of 10 y without ceasing.

Figure 7 summarizes the changes in the production rate for all 120 simulations. Depending on the transmissivity in the imaginary region, the production scenario for ten years varied from one maintaining the production rate without declining, to another with a steep decline to half of the initial value (Figure 7a). The frequency of the production rate occurred in the interval from 70 to 190 t/h (Figure 7b). As in the frequency distribution of pressure, the frequency of the production rate was higher near the upper limit, and it was distributed broadly toward the lower limit. By applying such a frequency distribution of production rates to the feasibility study of a real geothermal project, we will be able to determine expected income.

## 4. DEPENDENCIES ON CONDITIONS

### 4.1 Amplitude of Modifying Transmissivity Randomly

Finally, we investigated how the simulated frequency distribution of the production rate was affected by the modification of several conditions. Figure 8 shows a case with a smaller amplitude of modifying transmissivity randomly than that in Section 3.2.2. Thus, transmissivity was varied by two orders of magnitude, from $8.17 \times 10^{-9}$ to $8.17 \times 10^{-7}$ $m^3$ $Pa^{-1}$ $s^{-1}$. By reducing the amplitude, the frequency distribution became more sharply focused, with a narrower distribution. This results in underestimating risks to geothermal projects by neglecting the probability of pessimistic cases occurring with large declines in the production rate below 100 t/h. Sufficient large amplitude variations that include pessimistic cases are recommended in order to take into account reasonable project risks.

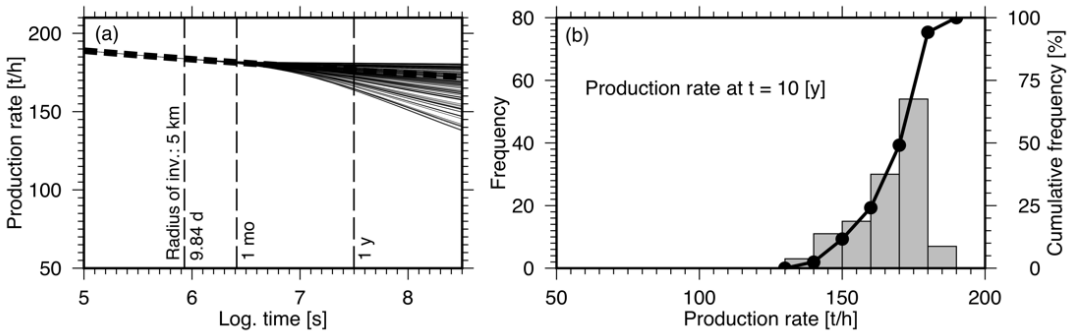


**Figure 8: Changes in the production rate with a constant wellhead pressure. The amplitude of modifying transmissivity in the imaginary region has been reduced. (a) Temporal changes for all 120 simulations. The thick broken line represents the probable case. (b) Frequency distribution at the end of all simulations (10 y).**

### 4.2 Dividing the Imaginary Region

The imaginary region was divided into two parts along the broken line 385 m (i.e., one grid interval) from the wellbore as illustrated in Figure 4. The transmissivity in each part was modified randomly and independently. Dividing the imaginary region into two parts resulted in the frequency distribution of the production rate becoming sharper and slightly narrower (Figure 9). This was because the probability of both imaginary regions having extremely large or small transmissivity values is smaller than that of a single imaginary region having extreme values. If conservative forecasts are preferred when analyzing practical problems, it appeared better to assume a single imaginary region in order to consider pessimistic cases with higher probability.

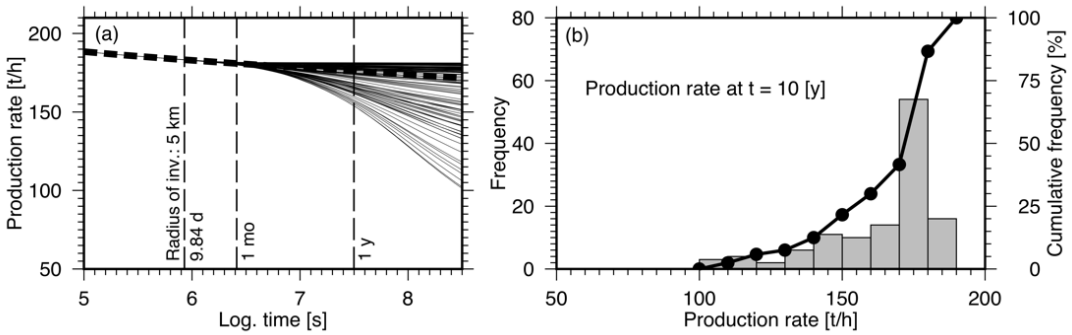


**Figure 9: Changes in the production rate with a constant wellhead pressure. The imaginary region was divided into two parts. (a) Temporal changes for all 120 simulations. The thick broken line represents the probable case. (b) Frequency distribution at the end of all simulations (10 y).**

### 4.3 Duration of the Production Test

Let us estimate how extending the duration of the production test improves the precision of forecasting the future production rate quantitatively. Figure 10 shows a case with a reservoir dimension extended from 10 to 27.0 km. In terms of the radius of investigation, this extension is equivalent to extending the duration of the production test from 9.84 d to 2.38 months. The transmissivity and storativity in the extended reservoir were equal to those of the original reservoir and fixed without modification. The precision of the forecast was effectively improved, with a doubling of the lower limit from 70 to 140 t/h and a reduction of the upper limit from 190 to 180 t/h.

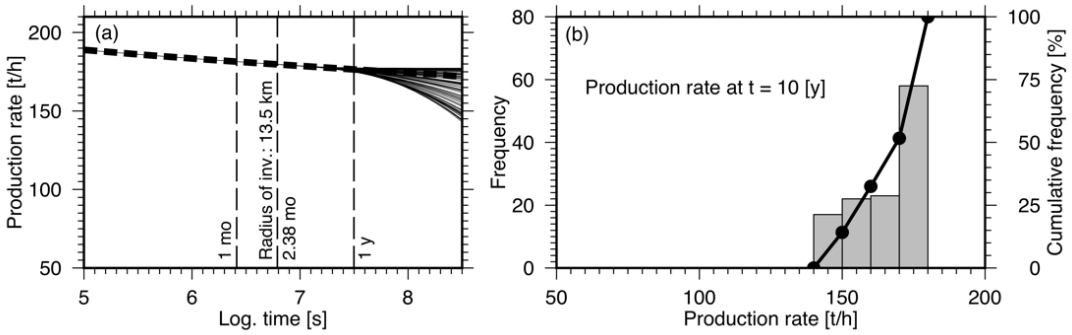


**Figure 10: Changes in the production rate with a constant wellhead pressure. The reservoir dimension was extended from 10 to 27.0 km. (a) Temporal changes for all 120 simulations. The thick broken line represents the probable case. (b) Frequency distribution at the end of all simulations (10 y).**

## 5. CONCLUSION

An approach was proposed for forecasting natural recharge to a reservoir during a long production period using pressure changes at the external reservoir boundary as well as at the feed zone of a production well. The transmissivity and storativity in the assumed imaginary region outside the reservoir control the natural recharge. Using a Monte Carlo approach, a case study assuming a planar reservoir successfully reproduced the proposed concept and generated frequency distributions of the pressure decline and production rate. The application of sufficiently large amplitudes in the random modifications of transmissivity is recommended in order to avoid missing the probability of pessimistic cases. If the imaginary region was divided into two parts, where transmissivity of each part was modified randomly and independently, the forecasted probability of extremely optimistic and pessimistic cases was slightly reduced. By extending the duration of the production test, the precision of forecasting the production rate was effectively improved.

## REFERENCES

Dake, L.P.: Fundamentals of Reservoir Engineering. Developments in Petroleum Science 8, Elsevier, Amsterdam (1978).

DiPippo, R.: Geothermal Power Plants: Principles, Applications, Case Studies and Environmental Impact, second ed. Butterworth-Heinemann, Oxford (2008).

Grant, M.A. and Bixley, P.F.: Geothermal Reservoir Engineering, second ed. Academic Press, Burlington (2011).

Matsumoto, M.: Connecting Wellbore and Reservoir Simulation Models Seamlessly Using a Highly Refined Grid, *Proceedings,* 43rd Workshop on Geothermal Reservoir Engineering, Stanford University, Stanford, CA (2018).